# Structure of a mixed dipolar liquid near a metal surface: A combined approach of weighted density and perturbative approximations

Sanjib Senapati and Amalendu Chandra
*Department of Chemistry, Indian Institute of Technology, Kanpur, India 208016*
(Received 12 January 2000)

We study the interfacial structure of a mixed dipolar liquid in contact with a metal surface by using a combined approach of the weighted density and the perturbative approximations. Both the molecular size and the dipole moment of various species can be unequal. The metal surface is treated by using the jellium model. Explicit numerical results are obtained for the interfacial structure of a binary dipolar liquid in contact with a metal surface of varying electron density. The theoretical predictions are compared with the results of Monte Carlo simulations and a good agreement is found for the inhomogeneous density, mole fraction, and polarization profiles of both the species in the interfacial region.

PACS number(s): 68.45.Da, 61.20.Gy

## I. INTRODUCTION

An understanding of the structure and dynamics of dipolar solvents in the vicinity of metal surfaces is extremely important for investigations of many electrochemical and surface processes. Many recent studies have investigated the structural properties of pure dipolar liquids near metal surfaces by means of analytical theories [1–7], computer simulations [8–17] and also experiments [18,19]. These studies have generated significant information about the spatial and orientational arrangement of dipolar molecules at metal-solvent interfaces. Several studies have also been carried out on the structure of ionic solutions near metal surfaces [20–31]. In contrast, relatively scant attention has been focused on the structure of mixed dipolar liquids near metal surfaces, despite the great importance of such interfaces in electrochemistry and surface science. In fact, we are not aware of any theoretical study on this problem. Consequently, the metal-fluid interfacial structure of dipolar mixtures is poorly understood. The structure of such an interface is expected to be much more complex than that of a pure solvent-metal interface because of selective adsoprtion of one species at the surface against the other. This selective adsorption can occur due to unequal molecular size and/or unequal polarity of different components of the mixed solvent. The purpose of the present paper is to present a theoretical study of this selective adsorption and the detailed microscopic structure of a metal-solvent interface involving a mixed dipolar liquid.

The present theory is based on a combined approach of the weighted density and the perturbative approximations for the isotropic and anisotropic parts of the solvent densities. Both the molecular sizes and the dipole moments of different components can be unequal. Explicit numerical results are obtained for the interfacial structure of a binary dipolar liquid in contact with a metal surface of varying free-electron density. The density profiles of both the solvent species are found to be highly inhomogeneous and oscillatory near the surface. The contact density of smaller molecules at the surface increases with an increase of surface electrostatic field. However, no such noticeable change of the contact density of bigger molecules is found which can be attributed to the larger contact distance and hence a weaker electrostatic field experienced by these molecules. The mole fraction profile also shows an oscillatory structure at the interface, indicating the presence of selective adsorption at the metal surface. The polarization profiles at the interface are found to depend nonlinearly with the electrostatic field of the metal and exhibits the presence of pronounced orientational order of dipolar molecules near the metal surface. This is most important in the first layer at the metal surface where the solvent dipoles tend to align parallel to the surface normal.

We have also carried out a Monte Carlo simulation of a binary dipolar mixture confined between two metal surfaces in order to verify the predictions of the present theory. The separation between the two metal surfaces is taken to be sufficiently large so that a bulk region of homogeneous density for both the species is found in the middle region of the simulation system. The theoretical predictions are compared with the results of Monte Carlo (MC) simulations and a good agreement is found for the inhomogeneous density, mole fraction, and polarization profiles of both the species in the interfacial region.

The organization of the rest of the paper is as follows. In Sec. II we present the theory and the details of Monte Carlo simulations are described in Sec. III. The numerical results are discussed in Sec. IV. Our conclusions are summarized in Sec. V.

## II. THEORY

We consider a dipolar mixture consisting of nonpolarizable dipolar molecules of $n$ different species. The molecules are confined between two metal surfaces. The solvent molecules are modeled as dipolar hard spheres where both the molecular diameter and the dipole moment of various species can be different and they interact through a short-range hard-sphere interaction and a long-range dipole-dipole interaction potential. The dipolar molecules also interact with the two metal surfaces. The interaction of the $i$th dipolar molecule of species $\alpha$ with the metal surfaces can be written as

$$u^{i}_{w;\alpha}(z_i,\Omega_i) = u'_{w;\alpha}(z_i,\Omega_i) + u''_{w;\alpha}(z_i,\Omega_i), \qquad (1)$$

 

where $u'$ and $u''$ represent the interaction with the walls located at $z=z'$ and $z=z''$, respectively. Both $u'$ and $u''$ include a short-range isotropic part and an electrostatic anisotropic part. The short-range isotropic part is described by a hard-wall–hard-sphere interaction and the anisotropic part represents the interaction of a dipole with the electrostatic field generated by nonuniform electron density of the metal surfaces. Thus, $u'_{w;\alpha}(z_i,\Omega_i)$ can be written as

$$u'_{w;\alpha}(z_i,\Omega_i)=u^{hw}_{w;\alpha}(|z_i-z'|)-E'(z_i)\cdot\mu^i_\alpha, \tag{2}$$

where $u^{hw}_{w;\alpha}(|z_i-z'|)$ is infinity for $|z_i-z'|<\sigma_\alpha/2$ and zero otherwise and $E'(z_i)$ is the electric field produced at $z_i$ by the surface charges of the metal wall located at $z'$. $\sigma_\alpha$ and $\mu_\alpha$ are, respectively, the diameter and dipole vector of a solvent molecule of species $\alpha$ with orientation $\Omega$.

We denote $\rho_\alpha(\mathbf{r},\Omega)$ as the position- and orientation-dependent number density of species $\alpha$ of the mixture. In density-functional theory (DFT), the grand potential of this system at fixed temperature, volume, external field, and chemical potential can be exactly expressed as a functional of the inhomogeneous density distribution

$$\overline{\Omega}[\rho_\alpha(\mathbf{r},\Omega)]=F[\rho_\alpha(\mathbf{r},\Omega)]+\sum_{\alpha=1}^{n}\int d\mathbf{r}\,d\Omega\,\rho_\alpha(\mathbf{r},\Omega)[u_{w;\alpha}(\mathbf{r},\Omega)-\overline{\mu}_\alpha], \tag{3}$$

where $u_{w;\alpha}(\mathbf{r},\Omega)$ is the interaction potential between a molecule of species $\alpha$ and the metal wall as given by Eqs. (1) and (2), $\overline{\mu}_\alpha$ is the chemical potential of species $\alpha$, and $T$ is the temperature. The intrinsic Helmholtz free energy $F[\rho_\alpha(\mathbf{r},\Omega)]$ is a universal functional of density and consists of two parts: an ideal part and an excess part. Minimizing the grand potential of Eq. (3) with respect to density and evaluating the chemical potential for the uniform mixture, one obtains the following expression for the equilibrium density of species $\alpha$ in presence of the metal surface:

$$\rho_\alpha(\mathbf{r},\Omega)=\frac{\rho^{(0)}_\alpha}{4\pi}\exp[-\beta^* u_\alpha(\mathbf{r},\Omega)+c^{(1)}_\alpha(\mathbf{r},\Omega;[\rho_\alpha(\mathbf{r},\Omega)])-c^{(1)}_\alpha(\rho^{(0)}_\alpha/4\pi)], \tag{4}$$

where $\beta^*=1/k_BT$, $k_B$ is the Boltzmann constant, $T$ is the temperature, $\rho^{(0)}_\alpha$ is the uniform bulk density of species $\alpha$, and $c^{(1)}_\alpha$ is the first-order direct correlation function which is given by the functional derivative of the excess free energy with respect to the density of species $\alpha$ [32]. The above equation is a formally exact relation which, in principle, may be solved for $\rho_\alpha(\mathbf{r},\Omega)$ if the functional $c^{(1)}_\alpha$ is known. In practice, however, $c^{(1)}_\alpha$ is generally unknown for inhomogeneous systems and so must be approximated. The simplest approximation of $c^{(1)}_\alpha(\mathbf{r},\Omega;[\rho_\alpha(\mathbf{r},\Omega)])$ of an inhomogeneous system involves a perturbative expansion (to first order) in terms of the density inhomogeneity which makes use of the second-order direct correlation function of the corresponding homogeneous system and is given by

$$c^{(1)}_\alpha(\mathbf{r},\Omega;[\rho_\alpha(\mathbf{r},\Omega)])-c^{(1)}_\alpha(\rho^{(0)}_\alpha/4\pi)=\sum_{\beta=1}^{n}\int d\mathbf{r}'\,d\Omega'\,\tilde{c}^{(2)}_{\alpha\beta}(\mathbf{r}-\mathbf{r}',\Omega,\Omega')\times\left(\rho_\beta(\mathbf{r}',\Omega')-\frac{\rho^{(0)}_\beta}{4\pi}\right), \tag{5}$$

where $\tilde{c}^{(2)}_{\alpha\beta}(\mathbf{r}-\mathbf{r}',\Omega,\Omega')$ is the second-order direct correlation function between species $\alpha$ and $\beta$ of the homogeneous mixture. The $z$-dependent first-order correlation function $c^{(1)}_\alpha(z,\Omega)$ can be obtained by integrating Eq. (5) over $x$ and $y$ coordinates. For convenience, we write $\tilde{c}^{(2)}_{\alpha\beta}(\mathbf{r}-\mathbf{r}',\Omega,\Omega')$ in terms of angular functions as follows:

$$\tilde{c}^{(2)}_{\alpha\beta}(\mathbf{r}-\mathbf{r}',\Omega,\Omega')=c^{000}_{\alpha\beta}(|\mathbf{r}-\mathbf{r}'|)+c^{110}_{\alpha\beta}(|\mathbf{r}-\mathbf{r}'|)\phi^{110}(\Omega,\Omega')+c^{112}_{\alpha\beta}(|\mathbf{r}-\mathbf{r}'|)\phi^{112}(\Omega,\Omega',\hat{r}), \tag{6}$$

where the angular functions $\phi^{110}(\Omega,\Omega')=(\hat{\mu}\cdot\hat{\mu}')$ and $\phi^{112}(\Omega,\Omega',\hat{r})=3(\hat{\mu}\cdot\hat{r})(\hat{\mu}'\cdot\hat{r})-(\hat{\mu}\cdot\hat{\mu}')$, $\hat{\mu}$ and $\hat{\mu}'$ are the unit vectors along dipole moments of particles located at $\mathbf{r}$ and $\mathbf{r}'$, and $\hat{r}=(\mathbf{r}-\mathbf{r}')/|\mathbf{r}-\mathbf{r}'|$. In Eq. (6), $c^{000}_{\alpha\beta}(|\mathbf{r}-\mathbf{r}'|)$ represents the isotropic or hard-sphere part and the second and third terms represent the anisotropic or dipolar parts of the intraspecies and interspecies direct correlation functions, whose analytical solutions are available within integral equation theories such as the mean spherical approximation (MSA) [33–35].

Alternatively, one can adopt the weighted density approximation (WDA) in which $c^{(1)}_\alpha(\mathbf{r},\Omega;[\rho_\alpha(\mathbf{r},\Omega)])$ for the inhomogeneous density is obtained by evaluating the corresponding expression $\tilde{c}^{(1)}_\alpha$ for the homogeneous fluid at an effective density $\overline{\rho}_\alpha(\mathbf{r},\Omega)$. Thus, we write

$$c^{(1)}_\alpha(\mathbf{r},\Omega;[\rho_\alpha(\mathbf{r},\Omega)])-c^{(1)}_\alpha(\rho^{(0)}_\alpha/4\pi)=\tilde{c}^{(1)}_\alpha(\overline{\rho}_\alpha(\mathbf{r},\Omega))-\tilde{c}^{(1)}_\alpha(\rho^{(0)}_\alpha/4\pi). \tag{7}$$

WDA has been shown to provide an accurate treatment for the hard-sphere correlation contributions [36–39]. In the spirit of earlier work [7,40,41], we decompose the total first-order direct correlation function into two parts: $c^{(1)}_\alpha=c^{(1)}_{\alpha;\mathrm{hs}}+c^{(1)}_{\alpha;\mathrm{ex}}$, where $c^{(1)}_{\alpha;\mathrm{hs}}$ is the isotropic hard-sphere contribution to the first-order direct correlation function and $c^{(1)}_{\alpha;\mathrm{ex}}$ represents the remaining anisotropic (or excess) contribution which arises from the explicit dipole-dipole electrostatic interactions and also from the coupling of electrostatic and hard-sphere interactions. We employ a combined approach in which we evaluate the isotropic hard-sphere contribution $c^{(1)}_{\alpha;\mathrm{hs}}$ using WDA and the remaining anisotropic part $c^{(1)}_{\alpha;\mathrm{ex}}$ through a perturbative approach by using an equation similar to Eq. (5) but involving only the anisotropic terms of the second-order direct correlation function.

Since the density inhomogeneity is only along the $z$ direction, the expressions for the density of the $\alpha$th species can now be written in the following form:

$$\rho_\alpha(z,\Omega)=\frac{\rho_{\alpha;\mathrm{hs}}(z)}{4\pi}\exp\Bigg[-\beta^* u_{w;\alpha}(z,\Omega)+\sum_{\beta=1}^{n}\int dx\,dy\,d\mathbf{r}'d\Omega'[c_{\alpha\beta}^{110}(|\mathbf{r}-\mathbf{r}'|;\rho^0)\phi^{110}(\Omega,\Omega')$$
$$+c_{\alpha\beta}^{(112)}(|\mathbf{r}-\mathbf{r}'|;\rho_0)\phi^{112}(\Omega,\Omega',\hat{r})][\rho_\beta(z',\Omega')-\rho_\beta^{(0)}/4\pi]\Bigg], \tag{8}$$

where

$$\rho_{\alpha;\mathrm{hs}}(z)=\rho_\alpha^{(0)}\exp\{\tilde{c}_{\alpha;\mathrm{hs}}^{(1)}[\overline{\rho}_{\alpha;\mathrm{hs}}(z)]-\tilde{c}_{\alpha;\mathrm{hs}}^{(1)}(\rho_\alpha^{(0)})\}. \tag{9}$$

Here $\tilde{c}_{\alpha;\mathrm{hs}}^{(1)}[\overline{\rho}_{\alpha;\mathrm{hs}}(z)]$ refers to the hard-sphere contribution to the first-order correlation function defined through WDA at an effective density $\overline{\rho}_{\alpha;\mathrm{hs}}(z)$, which is obtained as the weighted average

$$\overline{\rho}_{\alpha;\mathrm{hs}}(z)=\sum_{\beta=1}^{n}\int dz'\rho_{\alpha;\mathrm{hs}}(z')w_{\alpha\beta}[|z-z'|;\overline{\rho}_{\alpha;\mathrm{hs}}(z)].$$

The weight function $w_{\alpha\beta}(z-z')$ is calculated by following the prescription of Denton and Ashcroft [37]. In this scheme, the weight functions are specified first by normalization condition

$$\int d\mathbf{r}\,w_{\alpha\beta}(\mathbf{r})=1,\quad \alpha,\beta=1,2 \tag{10}$$

which ensures that the approximation is exact in the limit of a uniform mixture and second by requiring that the first functional derivatives of $\tilde{c}_{\alpha;\mathrm{hs}}^{(1)}$ with respect to the densities yield the exact two-particle direct correlation functions in the uniform limit. One then obtains the following analytic forms for the weight functions

$$w_{\alpha\beta}(\mathbf{r}-\mathbf{r}')=\frac{\tilde{c}_{\alpha\beta;\mathrm{hs}}^{(2)}(\mathbf{r}-\mathbf{r}')}{\partial\tilde{c}_{\alpha;\mathrm{hs}}^{(1)}/\partial\rho}. \tag{11}$$

The analytic solutions for the two-particle direct correlation functions of a uniform binary mixture of unequal sized hard spheres are available within the Percus-Yevick approximation. The expressions are given by [42,43]

$$\tilde{c}_{\alpha\alpha;\mathrm{hs}}^{(2)}(|\mathbf{r}-\mathbf{r}'|)=a_\alpha+b_\alpha|\mathbf{r}-\mathbf{r}'|+d'|\mathbf{r}-\mathbf{r}'|^3,\quad \alpha=1,2 \tag{12}$$

for $|\mathbf{r}-\mathbf{r}'|<\sigma_\alpha$ and zero otherwise, while

$$\tilde{c}_{\alpha\beta;\mathrm{hs}}^{(2)}(|\mathbf{r}-\mathbf{r}'|)=a_\gamma+\frac{\Theta(R)[bR^2+4\lambda d'R^3+d'R^4]}{|\mathbf{r}-\mathbf{r}'|}, \tag{13}$$

for $|\mathbf{r}-\mathbf{r}'|<\sigma_{12}$ and zero otherwise. Here $\Theta$ is the Heaviside step function, $\lambda=|\sigma_\alpha-\sigma_\beta|/2$, $R=|\mathbf{r}-\mathbf{r}'|-\lambda$, $\sigma_{12}=(\sigma_1+\sigma_2)/2$, and the $\gamma$ component refers to the species of smaller molecular diameter. The coefficients $a_\alpha$, $b_\alpha$, $b$, and $d'$ depend on the bulk densities of the two components and on the diameter ratio. The analytical expressions of these coefficients are given in the work of Ashcroft and Langreth [43]. The above expressions of the two-particle direct correlation functions lead to the following simplified expressions for the planar averaged weight functions $w_{\alpha\beta}(z)$ [37]

$$w_{11}(z)=\frac{\pi}{\partial\tilde{c}_1^{(1)}/\partial\rho}[a_1(\sigma_1^2-z^2)+\tfrac{2}{3}b_1(\sigma_1^3-z^3)+\tfrac{2}{5}d'(\sigma_1^5-z^5)],\quad z<\sigma_1 \tag{14}$$

$$w_{12}(z)=\frac{\pi}{\partial\tilde{c}_1^{(1)}/\partial\rho}[a_1(\sigma_{12}^2-z^2)+\tfrac{2}{3}b\sigma_1^3+2d'\lambda\sigma_1^4+\tfrac{2}{5}d'\sigma_1^5],\quad z<\sigma_{12} \tag{15}$$

$$w_{22}(z)=\frac{\pi}{\partial\tilde{c}_2^{(1)}/\partial\rho}[a_2(\sigma_2^2-z^2)+\tfrac{2}{3}b_2(\sigma_2^3-z^3)+\tfrac{2}{5}d'(\sigma_2^5-z^5)],\quad z<\sigma_2. \tag{16}$$

By integrating the above expressions of the two-particle hard-sphere direct correlation functions, one obtains explicit expressions of the density derivative $\partial\tilde{c}_{\alpha;\mathrm{hs}}^{(1)}/\partial\rho$ for $\alpha=1,2$. The one-particle hard-sphere correlation function $\tilde{c}_{\alpha;\mathrm{hs}}^{(1)}$ is then obtained by integrating $\partial\tilde{c}_{\alpha;\mathrm{hs}}^{(1)}/\partial\rho$ over density numerically by following the trapezoidal rule.

We expand the position- and orientation-dependent solvent density $\rho_\alpha(z,\Omega)$ in the basis set of spherical harmonics as follows [44,45]:

$$\rho_\alpha(z,\Omega)=\sum_{lm}a_{\alpha;lm}(z)Y_{lm}(\Omega), \tag{17}$$

so that the angle averaged density $\rho_\alpha(z)=\sqrt{4\pi}a_{\alpha;00}(z)$ and the polarization $P_\alpha(z)$ is related to $a_{\alpha;10}(z)$ by the following relation:

$$P_\alpha(z)=\sqrt{\frac{4\pi}{3}}\mu_\alpha a_{\alpha;10}(z). \tag{18}$$

We next substitute Eq. (17) and the explicit forms of the angular functions $\phi^{110}$ and $\phi^{112}$ into Eq. (8) and carry out the angular integrations to obtain the following simplified equations for the inhomogeneous solvent density and the polarization for the $\alpha$th species:

$$a_{\alpha;00}(z)=\frac{\rho_{\alpha;\mathrm{hs}}(z)}{\sqrt{4\pi}}\times\left[\frac{\sinh\{\beta^*\mu_\alpha E(z)+I_{\alpha;1}(z)+I_{\alpha;2}(z)\}}{\beta^*\mu_\alpha E(z)+I_{\alpha;1}(z)+I_{\alpha;2}(z)}\right], \tag{19a}$$

$$a_{\alpha;10}(z)=\left(\tfrac{3}{4}\right)^{1/2}\rho_{\alpha;\mathrm{hs}}(z)\times\left[\frac{\cosh\{\beta^*\mu_\alpha E(z)+I_{\alpha;1}(z)+I_{\alpha;2}(z)\}}{\beta^*\mu_\alpha E(z)+I_{\alpha;1}(z)+I_{\alpha;2}(z)}-\frac{\sinh\{\beta^*\mu_\alpha E(z)+I_{\alpha;1}(z)+I_{\alpha,2}(z)\}}{[\beta^*\mu_\alpha E(z)+I_{\alpha;1}(z)+I_{\alpha;2}(z)]^2}\right], \tag{19b}$$

for $z'+\sigma_\alpha/2<z<z''-\sigma_\alpha/2$ and $a_{\alpha;00}(z)=a_{\alpha;10}(z)=0$, otherwise. $E(z)$ is the total electrostatic field generated by the two metal surfaces and $I_{\alpha;1}(z)$ and $I_{\alpha;2}(z)$ are given by

$$I_{\alpha;1}(z)=\sum_{\beta=1}^{n}\int dz'\,a_{\beta;10}(z')c_{\alpha\beta}^{110}(z-z') \tag{20a}$$

and

$$I_{\alpha;2}(z)=\sum_{\beta=1}^{n}\int dx\,dy\,d\mathbf{r}'\,a_{\beta;10}(z')c_{\alpha,\beta}^{112}(|\mathbf{r}-\mathbf{r}'|)\times\left(\frac{3|z-z'|^2}{|\mathbf{r}-\mathbf{r}'|^2}-1\right), \tag{20b}$$

where $c_{\alpha\beta}^{110}(z-z')$ is obtained from $c_{\alpha\beta}^{110}(|\mathbf{r}-\mathbf{r}'|)$ by integrating over $x$ and $y$ coordinates. One can also derive an expression for the quantity $\langle\cos\theta_\alpha\rangle_z$, the average value of $\cos\theta_\alpha$ for a solvent molecule of species $\alpha$ at position $z$ from the surface. The expression of $\langle\cos\theta_\alpha\rangle_z$ is given by

$$\langle\cos\theta_\alpha\rangle_z=\mathcal{L}[\beta^*\mu_\alpha E+I_{\alpha;1}(z)+I_{\alpha;2}(z)], \tag{21}$$

where $\mathcal{L}$ refers to the Langevin function, defined as $\mathcal{L}(x)=\coth(x)-x^{-1}$. Equations (17)–(21) constitute a set of nonlinear equations for the calculation of the interfacial structure of a mixed dipolar solvent near a metal surface. The above equations can be solved iteratively once the metal electrostatic potential $E(z)$ is known. We note that $E(z)=-(\partial/\partial z)V(z)$, where $V(z)$ is the metal electrostatic potential which satisfies the Poisson equation

$$\frac{d^2}{dz^2}V(z)=-4\pi\rho_c(z), \tag{22}$$

where $\rho_c(z)$ is the charge density of the metal. An explicit modeling of the electronic structure of the metal is now necessary in order to calculate the charge density at the metal field. Following Berard *et al.* [1], we model the metal walls by semi-infinite jellium slabs of width $2z_w$. The jellium model consists of a uniform background of positive charge density $\rho_+$ which represents the metal nuclei and core electrons and the associated valence electron density $\rho_e(z)$. The valence electron density is calculated by using density functional theory [46,47]. In this approach, the electron density is calculated by solving the effective one-electron Schrödinger equation

$$-\frac{\hbar^2}{2m_e}\frac{d^2}{dz^2}\psi_n(z')+V_{\mathrm{eff}}(z')\psi_n(z')=\epsilon_n\psi_n(z'), \tag{23}$$

where $\psi_n$ and $\epsilon_n$ are the one-electron normalized eigenfunction and energy eigenvalues for the $n$th state and $m_e$ is the mass of an electron. $z'$ denotes the $z$ coordinate with origin at the center of the metal slab. $V_{\mathrm{eff}}(z')$ is the effective potential which is given by

$$V_{\mathrm{eff}}(z')=V_{\mathrm{jel}}(z')+V_{\mathrm{xc}}(z')+V_{\mathrm{dip}}(z'), \tag{24}$$

where $V_{\mathrm{jel}}(z')$ represents instantaneous interaction of an electron with the field of the jellium, $V_{\mathrm{xc}}(z')$ is the exchange and correlation potential, and $V_{\mathrm{dip}}(z')$ is the average interaction energy of the electron with the dipolar solvents. The valence electron density $\rho_e(z')$ is given by

$$\rho_e(z')=\frac{m_e}{\pi\hbar^2}\sum_{\epsilon_n<\epsilon_F}(\epsilon_F-\epsilon_n)|\psi_n(z')|^2, \tag{25}$$

where $\epsilon_F$ is the Fermi energy which is obtained from the following equation

$$\epsilon_F=\frac{2\pi\hbar^2\rho_+ z_w}{m_e n_F}+\sum_{\epsilon_n<\epsilon_F}\frac{\epsilon_n}{n_F}, \tag{26}$$

where $n_F$ is the number of eigenstates with energy $\epsilon_n<\epsilon_F$. Equation (26) is obtained by using the charge neutrality condition.

In the present work, we have used the local density approximation with Wigner's expression for the exchange and correlation energy [48]

$$V_{\mathrm{xc}}(z')=-e^2\left[\frac{0.611}{r_s(z')}+0.147\frac{4r_s(z')+23.4a_0}{[r_s(z')+7.8a_0]^2}\right], \tag{27}$$

where $r_s(z')=[4\pi\rho_e(z')/3]^{-1/3}$, $e$ is the magnitude of electronic charge, and $a_0$ is the Bohr radius. The interaction of an electron with the solvent dipoles is given by [1]

$$V_{\mathrm{dip}}(z')=\frac{2\pi e}{3}\sum_\alpha\rho_\alpha\mu_\alpha\left[\int_0^{z'}g_{w\alpha}^{011}(z)dz-\int_{z'}^{\infty}g_{w\alpha}^{011}(z)dz\right], \tag{28}$$

where $g_{w\alpha}^{011}(z)$ is the (011) component of the following Legendre polynomial expansion of the correlation function between the metal and the solvent species $\alpha$:

$$g_{w\alpha}(z,\theta)=\sum_n(-1)^n g_{w\alpha}^{011}(z)P_n(\cos\theta), \tag{29}$$

where $P_n(\cos\theta)$ is the Legendre polynomial of order $n$. Clearly, the metal potential depends on the structure of the dipolar mixture which, in turn, depends on the potential of the metal surface. Thus, the above equations for the metal potential and the solvent structure are solved self-consistently through iteration. Initially, the metal potential is calculated by replacing the dipolar mixture by vacuum. The dipolar mixture was then introduced and Eq. (19) was solved for the solvent density and polarization. After this initial calculation, $V_{\mathrm{dip}}(z')$ was evaluated using Eq. (28) and the new electron distribution was calculated by solving Eqs. (23) and (25). The metal potential was calculated from the new electron distribution by using Eq. (22) and the corresponding metal field was used in the next set of solutions of Eq. (19) and this iterative process was continued until convergence was attained.

The systems studied in this work are specified by the values of the following reduced parameters: the bulk density of species $\alpha$, $\rho_\alpha^* = \rho_\alpha \sigma_\alpha^3$; the dipole moment of a molecule of species $\alpha$, $\mu_\alpha^* = \sqrt{\mu_\alpha^2 / k_B T \sigma_\alpha^3}$; the molecular size ratio, $\Gamma = \sigma_2 / \sigma_1$; and the reduced Wigner-Seitz radius of the metal, $r_s^* = r_s / a_0$, where $a_0$ is the Bohr radius. In the numerical calculations, we have used three different values of $r_s^*$. The values of the other parameters characterizing the two solvent species are $\rho_1^* = 0.11$, $\rho_2^* = 0.63$, $\mu_1^* = 0.65$, $\mu_2^* = 1.29$, and $\Gamma = 1.5$. The results of the inhomogeneous density and polarization are discussed in terms of the reduced quantities: $\rho_\alpha(z)^* = \rho_\alpha(z)\sigma_\alpha^3$ and $P_\alpha(z)^* = P_\alpha(z)\sqrt{\sigma_\alpha^3 / k_B T}$.

## III. MONTE CARLO SIMULATIONS

The results computed with the theory described above are compared with those obtained from a Monte Carlo simulation of a dipolar mixture confined between two metal surfaces. The dipolar mixture is characterized by the same parameters as described above and the metal surface by reduced Wigner-Seitz radius $r_s^* = 2.65$. The separation between the two surfaces is taken to be large enough so that the solvation zone at one surface is not affected by the other and a region of homogeneous bulk density is obtained in the middle region of the simulated system. The simulation is carried out with a total of 256 molecules (93 of species 1 and 163 of species 2) in a rectangular box with dimension $L \times L \times h$, where $h$ is the separation between the walls and $L$ is the length of the central simulation box in $x$ and $y$ directions. The walls are located at $z = 0$ and $z = 10.5\sigma_1$ and the periodic boundary conditions are set at 0 and $9.1\sigma_1$ along $x$ and $y$ directions. This ensures a bulk region of homogeneous densities $\rho_1^* = 0.11$ and $\rho_2^* = 0.63$ in the middle region of the simulation system. In the simulation, the long-range dipolar interactions are treated by using the Ewald summation (slab adapted) method [49]. The Ewald parameters employed are the convergence parameter $\alpha / L = 6.4$, a reciprocal space cutoff of $15\sigma_1^{-1}$, and $\epsilon' = \infty$, where $\epsilon'$ is the dielectric constant of the medium that surrounds the infinite array of periodically replicated systems. The minimum image convention was used for the real-space portion of the Ewald sum.

Initially the electrostatic potential of the metal surfaces is calculated by replacing the dipolar mixture by vacuum. The dipolar molecules of the two species are then introduced and the system is equilibrated for 25 000 MC passes. The simulations are continued for another 25 000 MC passes and $g_{w\alpha}^{011}(z)$ is calculated. After this initial simulation, $V_{\mathrm{dip}}(z')$ is calculated using Eq. (28) and the new electron distribution is calculated by solving Eqs. (23) and (25). The metal potential is calculated from the new electron density by using Eq. (22) and the corresponding metal field is used in the next simulation run. This iterative process is continued until convergence is reached. After convergence, the simulation is continued for another 50 000 MC passes for the calculation of the interfacial structure. The number densities of the two solvent species are calculated by computing the average number of molecules in slabs of thickness $\Delta z = 0.02\sigma_1$. The orientational structure of solvent molecules are calculated by finding the solvent polarization along the field direction ($z$) which is obtained by calculating the total dipole moment along the $z$ direction in different slabs at various distances from the solid surfaces.

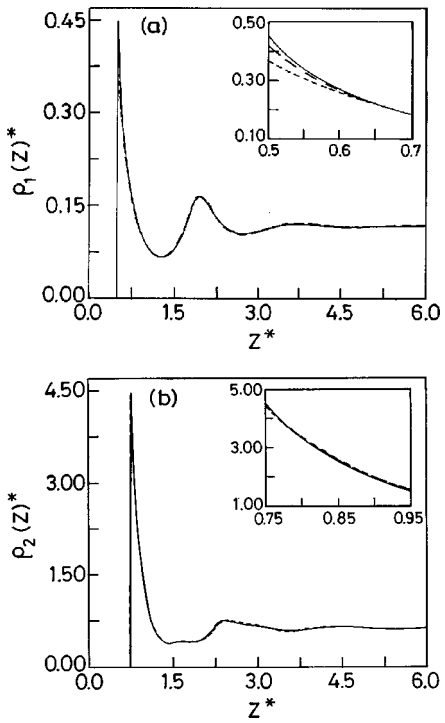


FIG. 1. The variation of reduced number density of (a) species 1 and (b) species 2 with distance from the metal surface. The solid, long dashed, and short dashed curves are for $r_s^* = 2.65$, 3.0, and $\infty$, respectively. The reduced distance $z^* = z/\sigma_1$. Other reduced quantities are defined in the text. The inset shows the solvent densities near the metal surface.

## IV. NUMERICAL RESULTS

In Fig. 1 we have shown the results of the density profiles of the two solvent components near a metal surface for three different values of the reduced Wigner-Seitz radius $r_s^* = 2.65$, 3.0, and $\infty$. We note that $r_s^* = \infty$ corresponds to a nonmetallic or an inert surface. It is seen that the density profiles of both the species are highly nonuniform near the metal surface. Also, the density of species 1 at the surface increases slightly with decrease of $r_s^*$ which is more clearly shown in the inset of Fig. 1(a). However, no noticeable change in the contact density of species 2 is observed with the decrease of $r_s^*$. The metal electrostatic field at the surface increases with the decrease of $r_s^*$. The molecules of species 2 are bigger and thus cannot come as close to the metal as the smaller molecules of the first species 1. As a result, the interfacial molecules of species 2 experience a weaker field of the metal and hence shows no change of contact density with the decrease of $r_s^*$. Also, the profiles of $\rho_\alpha(z)^*$ show pronounced oscillations in the interfacial region indicating layering of the solvent structure at microscopic level induced by the metal field.

We next discuss the results of the polarizations of the two components which are shown in Fig. 2. The solvent polarizations are found to be most significant near the surface and then they oscillate until the bulk values are reached. The results of both the species seem to depend rather strongly on

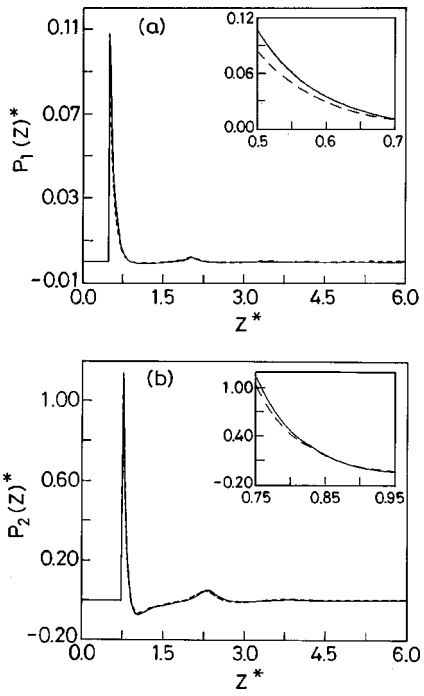


FIG. 2. The variation of reduced solvent polarization of (a) species 1 and (b) species 2 with distance from the metal surface. The solid and dashed curves are for $r_s^*=2.65$ and 3.0, respectively. The inset shows the solvent polarization near the metal surface.

the strength of the metal field characterized by the value of $r_s^*$. Also, the polarization increases with the decrease of $r_s^*$ in a nonlinear fashion. In Fig. 3 we have plotted the quantity $\langle \cos \theta_\alpha \rangle_z$ against $z$ for two different values of the Wigner-Seitz radius $r_s^*$. We note that there is no polarization for $r_s^*=\infty$ and hence $\langle \cos \theta \rangle_z$ is zero for this particular value of

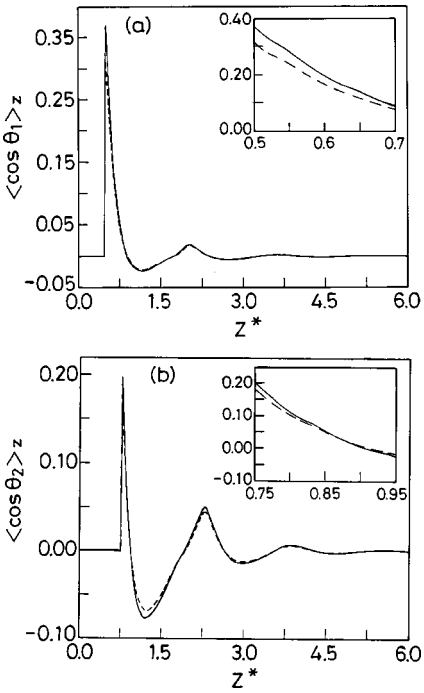


FIG. 3. The variation of $\langle \cos \theta_\alpha \rangle_z$ of (a) species 1 and (b) species 2 with distance. The different curves are as in Fig. 2. The inset shows the values of $\langle \cos \theta_\alpha \rangle_z$ near the metal surface.

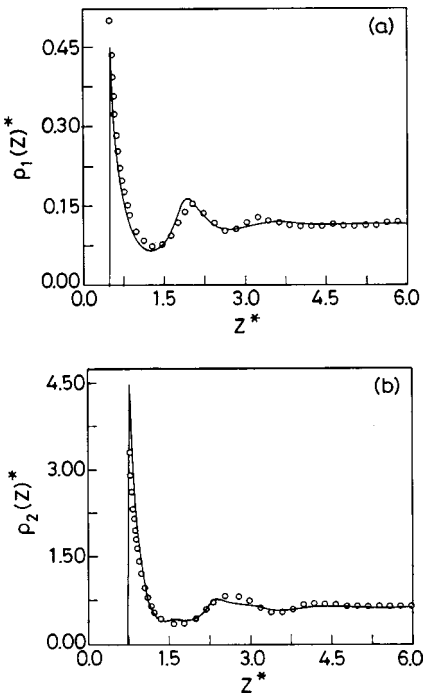


FIG. 4. Comparison of the theoretical and Monte Carlo simulation results of the density profiles of (a) species 1 and (b) species 2 of a dipolar mixture in contact with a metal surface characterized by $r_s^*=2.65$. The solid curve represents the results of present theory and the circles represent the simulation results. The values of other parameters are the same as in Fig. 1.

$r_s^*$. For smaller values of $r_s^*$, the molecules near the surface are found to be significantly oriented.

In Fig. 4 we have compared the theoretical and simulation results of the density profiles of species 1 and 2 at metal-solvent interface for $r_s^*=2.65$. In Fig. 5 we have compared the results for the polarizations of the two components. Finally, in Fig. 6 we have compared the results of the mole fraction of species $1[x_1=\rho_1/(\rho_1+\rho_2)]$ at various distances from the metal surface. The profile of the mole fraction reveals the extent of selective adsorption at the metal surface. It is seen that the overall agreement between the theoretical and the simulation results is quite good. Especially, the oscillatory and layered structure of the density, polarization, and mole fraction profiles in the interfacial region is correctly predicted by the present theory. We note that the present theory predicts a very small rise in the density of bigger molecules at around $z\approx 1.6$ which is not observed in the simulation. This small discrepancy can arise from the use of the weighted density approximation for the isotropic densities because a similar small rise in the density profile of bigger molecules was also observed in an earlier WDA-based study [50] of the structure of binary hard spheres near a hard wall at similar densities.

## V. SUMMARY AND CONCLUSIONS

We have carried out a theoretical study of the spatial and orientational structure of a mixed dipolar liquid in contact with a metal surface. The metal is treated by using the jellium model and quantum density functional theory. Our approach to the interfacial structure of the dipolar mixture is

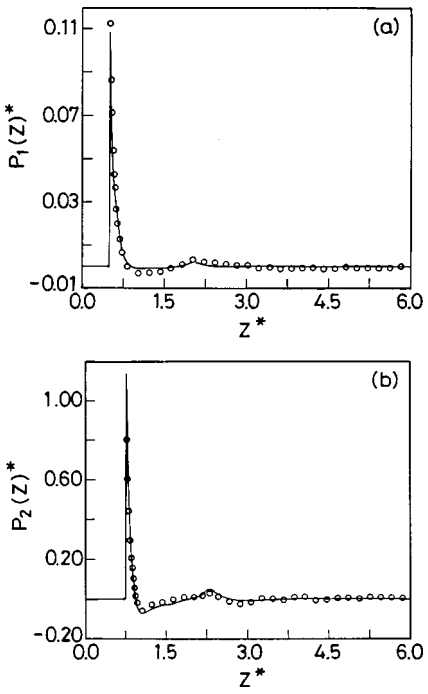


FIG. 5. Comparison of the theoretical and Monte Carlo simulation results of the polarization profiles of (a) species 1 and (b) species 2 of a dipolar mixture in contact with a metal surface. The values of the various parameters are the same as in Fig. 4.

based on a weighted density approximation for the isotropic part of the solvent density and the anisotropic (or dipolar) part is calculated by using a perturbative approach. The theory, however, retains the nonlinear dependence of the interfacial solvent density and polarization on the metal electrostatic potential and the intraspecies and interspecies solvent-solvent interactions. The metal potential arises from the inhomogeneous electron density at the surface which is influenced by the solvent mixture and the solvent structure, in turn, is influenced by the metal and the entire system is solved self-consistently until convergence is attained. It is found that the number densities of both the species near the metal surface are highly nonuniform and oscillatory. The contact density of smaller molecules at the surface increases with an increase of surface electrostatic field. However, no such change of the contact density of bigger molecules is found which can be attributed to the larger contact distance of these molecules from the metal surface. The profile of mole fraction of a component also shows highly oscillatory structure indicating the presence of selective adsorption at the metal surface. The polarization profiles at the interface are found to depend nonlinearly with the electrostatic field of the metal and exhibits the presence of pronounced orientational order of dipolar molecules near the metal surface. This is most important in the first layer at the metal surface where

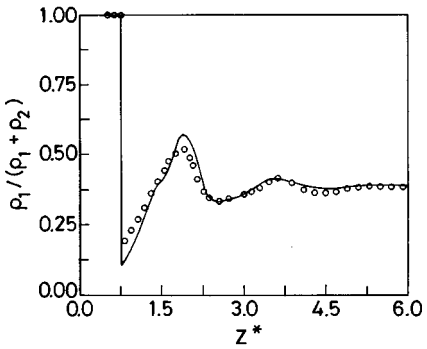


FIG. 6. Comparison of the theoretical and simulation results of the mole fraction profile of species 1. The values of the various parameters are the same as in Fig. 4.

the solvent dipoles tend to align parallel to the surface normal. The theoretical predictions are compared with the results of the MC simulations and a good agreement is found for the inhomogeneous density, mole fraction, and polarization profiles of both the species in the interfacial region.

Although we are not aware of any experimental study on the structure of mixed solvents near metal surfaces, there have been a few experimental studies on the spatial and orientational structure of water and aqueous ionic solutions near charged metal surfaces [18,19,29–31]. Toney and coworkers [18,19] measured the distribution of water molecules near silver surfaces by means of *in situ* x-ray scattering. They found that the water density near the surface is significantly higher than the bulk density. The density profile was found to be oscillatory in the vicinity of the metal surface. Also, pronounced orientational structure was found for interfacial molecules. Similar orientational ordering was also observed in other experiments [29,30]. However, the degree of orientational ordering found in these studies was significantly higher than the predictions of the present theory which can be attributed to the surface charges of the metal surfaces used in the experiments. The metal surface considered in the present theory is uncharged. It would certainly be worthwhile to generalize the present theory to calculate the solvent structure near a charged metal surface.

The theoretical study presented here can also be extended to more complex interfaces. For example, it will be interesting to study the structure of electrolyte solutions near a charged metal surface. The role of selective adsorption in solvation at a metal-solvent interface is another important issue which is not yet investigated. Work in these directions is in progress.

## ACKNOWLEDGMENT

The financial support of the Council of Scientific and Industrial Research (CSIR), Government of India, is gratefully acknowledged.

[1] D. Berard, M. Kinoshita, X. Ye, and G. N. Patey, J. Chem. Phys. **101**, 6271 (1994).

[2] R. Akiyama and F. Hirata, J. Chem. Phys. **108**, 4904 (1998).

[3] M. Yamamoto and M. Kinoshita, Chem. Phys. Lett. **274**, 513 (1997).

[4] J. P. Badiali, M. L. Rosinberg, and J. Goodisman, J. Electroanal. Chem. Interfacial Electrochem. **130**, 31 (1981).

[5] I. Benjamin, in *Modern Aspects of Electrochemistry*, edited by J. O'M. Bockris, B. E. Conway, and R. E. White (Plenum, New York, 1995).

[6] R. R. Nazmutdinov, M. Probst, and K. Heinzinger, J. Electroanal. Chem. **369**, 227 (1994).
[7] S. Senapati and A. Chandra, Phys. Rev. E **59**, 3140 (1999).
[8] J. C. Shelley, G. N. Patey, D. R. Berard, and G. M. Torrie, J. Chem. Phys. **107**, 2122 (1997).
[9] J. I. Siepmann and M. Sprik, J. Chem. Phys. **102**, 511 (1995).
[10] J. Hautman, J. W. Halley, and Y.-J. Rhee, J. Chem. Phys. **91**, 467 (1989).
[11] E. Spohr, J. Chem. Phys. **107**, 6342 (1997); J. Phys. Chem. **93**, 6171 (1989).
[12] A. Kohlmeyer, W. Witschel, and E. Sphor, Chem. Phys. **213**, 211 (1996).
[13] K. Foster, K. Raghavan, and M. Berkowitz, Chem. Phys. Lett. **162**, 32 (1989); **177**, 426 (1991).
[14] K. Raghavan, K. Foster, K. Motakabbir, and M. Berkowitz, J. Chem. Phys. **94**, 2110 (1991).
[15] X. Xia and M. Berkowitz, Phys. Rev. Lett. **74**, 3193 (1995).
[16] M. R. Philpott, J. N. Glosli, and S. Zhu, Surf. Sci. **335**, 422 (1995).
[17] A. Chandra and S. Senapati, J. Mol. Liq. **77**, 77 (1998).
[18] M. F. Toney, J. N. Howard, J. Richer, G. L. Borges, D. C. Wielser, D. Yee, and L. B. Sorensen, Nature (London) **368**, 444 (1994).
[19] M. F. Toney, J. N. Howard, J. Richer, G. L. Borges, J. G. Gordon, O. R. Melroy, D. G. Wiesler, D. Yee, and L. B. Sorensen, Surf. Sci. **335**, 326 (1995).
[20] D. R. Berard, M. Kinoshita, N. M. Cann, and G. N. Patey, J. Chem. Phys. **107**, 4719 (1997).
[21] S.-B. Zhu and M. R. Philpott, J. Chem. Phys. **100**, 6961 (1994).
[22] W. Schmickler and D. Henderson, J. Chem. Phys. **80**, 3381 (1984).
[23] J. W. Halley and D. Price, Phys. Rev. B **35**, 9095 (1987); **38**, 9357 (1988).
[24] I. Yeh and M. Berkowitz, Chem. Phys. Lett. **301**, 81 (1999).
[25] E. Spohr, J. Mol. Liq. **64**, 91 (1995).
[26] D. Berard, M. Kinoshita, X. Ye, and G. N. Patey, J. Chem. Phys. **102**, 1024 (1995).
[27] D. A. Rose and I. Benjamin, J. Chem. Phys. **95**, 6856 (1991); **98**, 2283 (1993).
[28] J. P. Badiali, M. L. Rosinberg, F. Varicat, and L. Blum, J. Electroanal. Chem. Interfacial Electrochem. **158**, 253 (1983).
[29] K. Ataka, T. Yotsuyanagi, and M. Osawa, J. Phys. Chem. **100**, 10 664 (1996).
[30] J. D. Porter and A. S. Zinn, J. Phys. Chem. **97**, 1190 (1993).
[31] J. Wang and B. M. Ocko, Phys. Rev. B **46**, 10 321 (1992).
[32] J. P. Hansen and I. R. McDonald, *Theory of Simple Liquids* (Academic, London, 1986).
[33] M. S. Wertheim, J. Chem. Phys. **55**, 4291 (1971).
[34] S. A. Adelman and J. M. Deutch, J. Chem. Phys. **59**, 3971 (1973).
[35] D. Isbister and R. J. Bearman, Mol. Phys. **28**, 1297 (1974).
[36] P. Tarazona, Phys. Rev. A **31**, 2672 (1985); **32**, 3148 (1985).
[37] A. R. Denton and N. W. Ashcroft, Phys. Rev. A **44**, 8242 (1991); **39**, 426 (1989).
[38] W. A. Curtin and N. W. Ashcroft, Phys. Rev. A **32**, 2909 (1985).
[39] C. N. Patra and S. K. Ghosh, Phys. Rev. E **49**, 2826 (1994).
[40] C. N. Patra and S. K. Ghosh, J. Chem. Phys. **106**, 2752 (1997).
[41] D. Das, S. Senapati, and A. Chandra, J. Chem. Phys. **110**, 8129 (1999); S. Senapati and A. Chandra, J. Chem. Phys. (to be published).
[42] J. L. Lebowitz, Phys. Rev. **133**, A895 (1964).
[43] N. M. Ashcroft and D. C. Langreth, Phys. Rev. **156**, 685 (1967).
[44] B. Bagchi and A. Chandra, Adv. Chem. Phys. **80**, 1 (1991).
[45] C. G. Grey and K. Gubbins, *Theory of Molecular Fluids* (Clarendon, Oxford, 1984).
[46] P. Hohenberg and W. Kohn, Phys. Rev. **136**, B864 (1964).
[47] W. Kohn and L. J. Sham, Phys. Rev. **140**, A1133 (1965).
[48] E. Wigner, Phys. Rev. **36**, 1002 (1934).
[49] J. Shelley and G. N. Patey, Mol. Phys. **88**, 385 (1996).
[50] Z. Tan, U. M. B. Marconi, F. van Swol, and K. E. Gubbins, J. Chem. Phys. **90**, 3704 (1989).